JGR Earth Surface

RESEARCH ARTICLE
10.1029/2018JF004815

Fan-Surface Evidence for Debris-Flow Avulsion Controls and Probabilities, Saline Valley, California

T. de Haas[1,2], A. L. Densmore[1], T. den Hond[2], and N. J. Cox[1]

[1]Department of Geography, Durham University, Durham, UK, [2]Department of Physical Geography, Universiteit Utrecht, Utrecht, The Netherlands

Key Points:
- Debris-flow avulsions are mainly caused by thick lobes plugging the main channel
- Channel-bed superelevation can be large on debris-flow fans and is a weak indicator for avulsion
- A spatial framework of debris-flow lobe dimensions and channel depths can be used to predict avulsion locations and probabilities

Correspondence to:
T. de Haas,
T.deHaas@uu.nl

Citation:
de Haas, T., Densmore, A. L., den Hond, T., & Cox, N. J. (2019). Fan-surface evidence for debris-flow avulsion controls and probabilities, Saline Valley, California. *Journal of Geophysical Research: Earth Surface*, *124*, 1118–1138. https://doi.org/10.1029/2018JF004815

Received 17 JUL 2018
Accepted 30 MAR 2019
Accepted article online 4 APR 2019
Published online 7 MAY 2019

Abstract Debris-flow fans form by shifts of the active channel, termed avulsions. Field and experimental evidence suggest that debris-flow avulsions may be induced by depositional lobes that locally plug a channel or superelevation of the channel bed above the surrounding fan surface, by analogy to fluvial fans. To understand debris-flow avulsion processes, we differentiate between these controls by quantifying the spatial distribution of debris-flow lobe and channel dimensions, along with channel-bed superelevation, on nine debris-flow fans in Saline Valley, California, USA. Channel beds are generally superelevated by 2–5 channel depths above the fan surface, and locally by more than 7 channel depths, thereby substantially exceeding superelevation on fluvial fans. Depositional-lobe thickness and channel depth decrease with distance from the fan apex, although both are highly variable across the fans. Median channel depths roughly correspond to the 50th–75th percentiles of lobe thicknesses, while minimum channel depths roughly correspond to the 10th–25th percentiles. In contrast, the thicknesses of lobes that have triggered avulsions roughly equal local channel depths and are on average twice as thick as the local median lobe thickness. The spatial correspondence between avulsion locations and thick lobe deposits, and the lack of correlation with channel-bed superelevation, leads us to infer that avulsions on these fans are mostly caused by thick lobes forming channel plugs. Although results may vary with climatic and tectonic setting, our findings indicate that avulsion hazard assessment on populated fans should include mapping and monitoring of channel depths relative to typical deposit thicknesses on a given fan.

1. Introduction

Debris flows are common geomorphic processes in mountainous regions worldwide (e.g., Iverson, 1997; Takahashi, 1978). Deposition of sediment by repeated debris flows results in the formation of debris-flow fans where channels emerge from confined catchments into areas of local accommodation (Beaty, 1963; Blair & McPherson, 1994; De Haas et al., 2014; De Haas, Kleinhans, et al., 2015; Harvey, 2011; Hooke, 1967; Ventra & Nichols, 2014). Debris-flow fans owe their characteristic semiconical form to shifts of the active channel and locus of deposition in space and time, termed avulsions (e.g., De Haas et al., 2016; De Haas, Densmore, et al., 2018; Schumm et al., 1987; Schürch et al., 2016; Whipple & Dunne, 1992).

Understanding the processes and associated erosional and depositional patterns that lead to debris-flow avulsion is important for determining the spatiotemporal evolution of debris-flow fans, both for effective hazard mitigation and for reconstructing past environmental conditions. Owing to their moderate surface gradients and relatively low frequency of activity, debris-flow fans are preferred sites for settlements in mountainous areas (e.g., Jakob, 2005), and debris flows therefore pose a large threat to people, settlements, and infrastructure (e.g., Dowling & Santi, 2014; Iverson, 2014; Wieczorek et al., 2001). Debris-flow avulsions can be particularly dangerous, because mitigation measures in the active channel may not be able to reduce risk on other areas of the fan after avulsion (De Haas, Densmore, et al., 2018; De Haas, Kruijt, et al., 2018; Pederson et al., 2015). In addition, debris-flow fan deposits are archives of past flow processes (e.g., De Haas, Braat, et al.,2015; Dühnforth et al., 2007; Whipple & Dunne, 1992) and sediment supply (e.g., Dietrich & Krautblatter, 2017; Franke et al., 2015; McDonald et al., 2003), and they may therefore record sedimentary signals of past climate changes (e.g., D'Arcy et al., 2017). The frequency of avulsion determines the revisiting time of each location on the fan surface, and thus the utility of the surface in recording past environmental conditions (e.g., Dühnforth et al., 2007).

De Haas, Densmore, et al. (2018) analyzed the spatiotemporal patterns of debris-flow fan evolution based on direct field observations (Imaizumi et al., 2016; Suwa & Okuda, 1983; Wasklewicz & Scheinert, 2016)

and reconstructions of debris-flow deposition (e.g., Bollschweiler et al., 2008; Dühnforth et al., 2008; Helsen et al., 2002; Stoffel et al., 2008; Schürch et al., 2016; Zaginaev et al., 2016). They identified two important controls on debris-flow avulsion that operate over separate time scales. First, on the time scale of individual flows, deposition of debris-flow lobes may locally plug channels, promoting avulsion in subsequent flows (Whipple & Dunne, 1992). Second, the average locus of debris-flow deposition gradually shifts toward topographically lower parts on a fan over longer, but poorly constrained, time scales that are on the order of tens of events (De Haas, Densmore, et al., 2018). Limited observations on natural debris-flow fans (De Haas, Densmore, et al., 2018; Suwa & Okuda, 1983; Suwa et al., 2009) and physical scale experiments (De Haas, Kruijt, et al., 2018) show that there is a strong relationship between avulsion occurrence and the sequence of flow sizes. In general, following the formation of a channel plug, small- to medium-sized debris flows leave deposits that step back sequentially toward the fan apex, until an event occurs that is sufficiently large to overtop these deposits and avulse out of the active channel. Beyond this general association, however, the precise ways in which debris-flow avulsions develop, and the characteristics of flows that can block channels and thus trigger avulsion, have not been described. It is therefore difficult to understand if and how avulsion locations can be predicted, or to develop a model for avulsion occurrence (e.g., McDougall, 2016).

One possibility is that plug deposition is the dominant control on avulsion occurrence. While this is not a new idea (e.g., Whipple & Dunne, 1992), it has not been well tested because we lack systematic data on the sizes of sediment plugs relative to the channels that they block, the locations at which plugs are most likely to form, and the characteristics of the plugs themselves, including their grain size. Plug deposition is a complex process that depends on debris-flow runout, volume, grain size, and water content as well as the geometry of the channel (De Haas, Densmore, et al., 2018; De Haas, Kruijt, et al., 2018; Whipple & Dunne, 1992). In the absence of detailed field data on most of these parameters, we hypothesize that whether a channel plug is able to sufficiently block a channel to force avulsion depends on the size of the deposit in relation to the channel dimensions. If this is true, then the relationship between lobe and channel dimensions across a fan surface may inform us about future avulsion sites. On a fluvially dominated alluvial fan, Stock et al. (2008) found a decrease in hydraulic channel radius with distance from the fan apex, but how channel dimensions vary on debris-flow fans is currently unknown. An additional unknown is what determines lobe dimensions and runout. Previous research suggests that debris-flow volume, water content, and grain-size distribution may affect lobe dimensions and runout (e.g., Berti & Simoni, 2007; De Haas, Braat, et al., 2015; Griswold & Iverson, 2008; Major, 1997; Major & Iverson, 1999; Whipple & Dunne, 1992). Both Major and Iverson (1999) and De Haas et al. (2015) experimentally found that debris-flow lobe thickness and runout may strongly depend on the grain-size distribution at the debris-flow front, which may thereby exert a control on the avulsion processes on debris-flow fans. However, to test this hypothesis, an extensive survey of debris-flow lobe grain sizes across a fan surface would be required.

Alternatively, the probability of avulsion may depend mostly on the superelevation of an active channel bed—that is, the height difference or relief between the channel bed and the minimum elevation of the interfluve surface, outside of the channel levee. Note that here we adopt the term superelevation by analogy with fluvial fans and that this term should not be confused with the increase in flow surface level at the outer bends of debris-flow and fluvial channels to which the phrase is also commonly applied (e.g., Dietrich et al., 1979; Scheidl et al., 2014). Field, experimental, and modeling data from fluvial fans suggest that avulsion generally occurs once the active channel bed has aggraded by approximately 0.5 to 1 channel depth above the surrounding floodplain (e.g., Carling et al., 2016; Jerolmack & Mohrig, 2007; Mohrig et al., 2000). Such a relationship is useful for avulsion prediction, because it yields a characteristic avulsion time scale if the aggradation rate is known. However, debris flows and fluvial flows have different rheologies and sediment-load characteristics and therefore might have characteristically different superelevation ranges. Therefore, to assess whether superelevation is a critical control of avulsion on debris-flow fans, we should first understand whether there is a correlation between superelevation and avulsion occurrence, or alternatively whether debris-flow and fluvial fan avulsions occur in response to different controls.

To effectively predict debris-flow avulsions, we thus have to identify the dominant mode of avulsion and the conditions under which they occur. Limited channel-bed superelevation, in the range of ~1 channel depth as observed on many fluvial fans, and no clear relationship between the occurrence of thick lobes and avulsion locations would point to channel-bed superelevation as a predominant control and means to predict avulsion on debris-flow fans. In that case, the spatial distribution of local superelevation values would be a key data set to inform avulsion likelihood. In contrast, high channel-bed superelevations and a strong

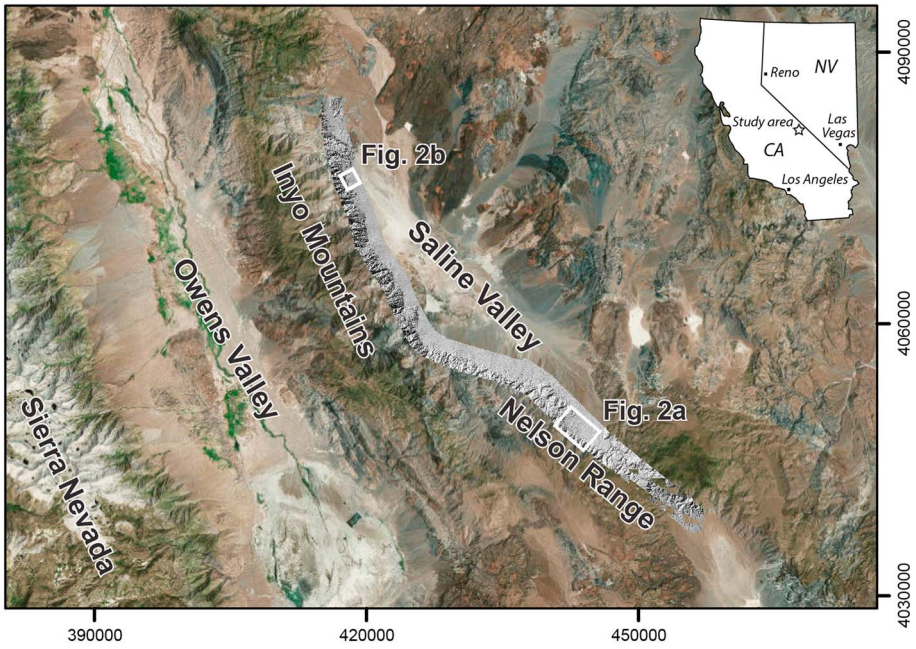

Figure 1. Overview of Saline Valley, California, USA, and locations of the fans studied. The gray area shows a hillshaded image of the lidar elevation data set along the western margin of Saline Valley. Coordinates are in UTM zone 11N, datum WGS84.

relationship between thick lobes and avulsion locations would indicate that the spatial distributions of lobe and channel dimensions, and the resulting likelihood of channel-plug formation, are the predominant controls on avulsion locations and probabilities. In that case, the distributions of lobe and channel dimensions across a fan surface could be combined to predict avulsion likelihood.

Here, we evaluate both of these avulsion controls by measuring debris-flow lobe and channel dimensions as well as channel-bed superelevation on the surfaces of nine remarkably well-preserved debris-flow fans in Saline Valley, California, USA (Figures 1 and 2). Our goals are to (1) quantify debris-flow lobe dimensions across a range of fan surfaces and compare these with channel dimensions at recognized avulsion locations; (2) quantify debris-flow lobe grain-size distributions across a fan surface and evaluate their impact on debris-flow lobe dimensions and runout, and thus on avulsion likelihood; (3) quantify the pattern of channel-bed superelevation and test its usefulness as a predictor of avulsion locations; and (4) evaluate the relative importance of these different avulsion controls. To our knowledge, this is the first systematic attempt to quantify lobe and channel dimensions and evaluate potential avulsion controls across a range of fan surfaces. Our aim, therefore, is both to evaluate avulsion controls and to collate the fan-surface data that would be needed to inform future avulsion models, although the derivation of such models is beyond the scope of this contribution.

This paper is structured as follows. We first describe the geologic, geomorphic, and present-day climatic setting of the study area. Then we detail the materials and methods. Subsequently, we present the general fan morphology, spatial trends in debris-flow lobe and channel dimensions, the debris-flow runout distribution, the relations between channel-plug thickness and median lobe thickness and channel depth, channel-bed superelevation, and spatial trends in debris-flow lobe grain-size distribution, as well as the relation between grain-size distribution and debris-flow lobe dimensions. Finally, we discuss implications for debris-flow avulsion mechanisms and hazard mitigation.

2. Study Area

2.1. Geologic and Geomorphic Setting

Saline Valley is a closed, terminal fault-bounded basin in eastern California (Oswald & Wesnousky, 2002). The study fans were selected for their pristine debris-flow depositional morphology, with very little evidence for reworking of the surfaces by fluvial and other secondary processes, which enables relatively precise measurement of debris-flow lobe and channel dimensions as well as the grain size of surficial deposits.

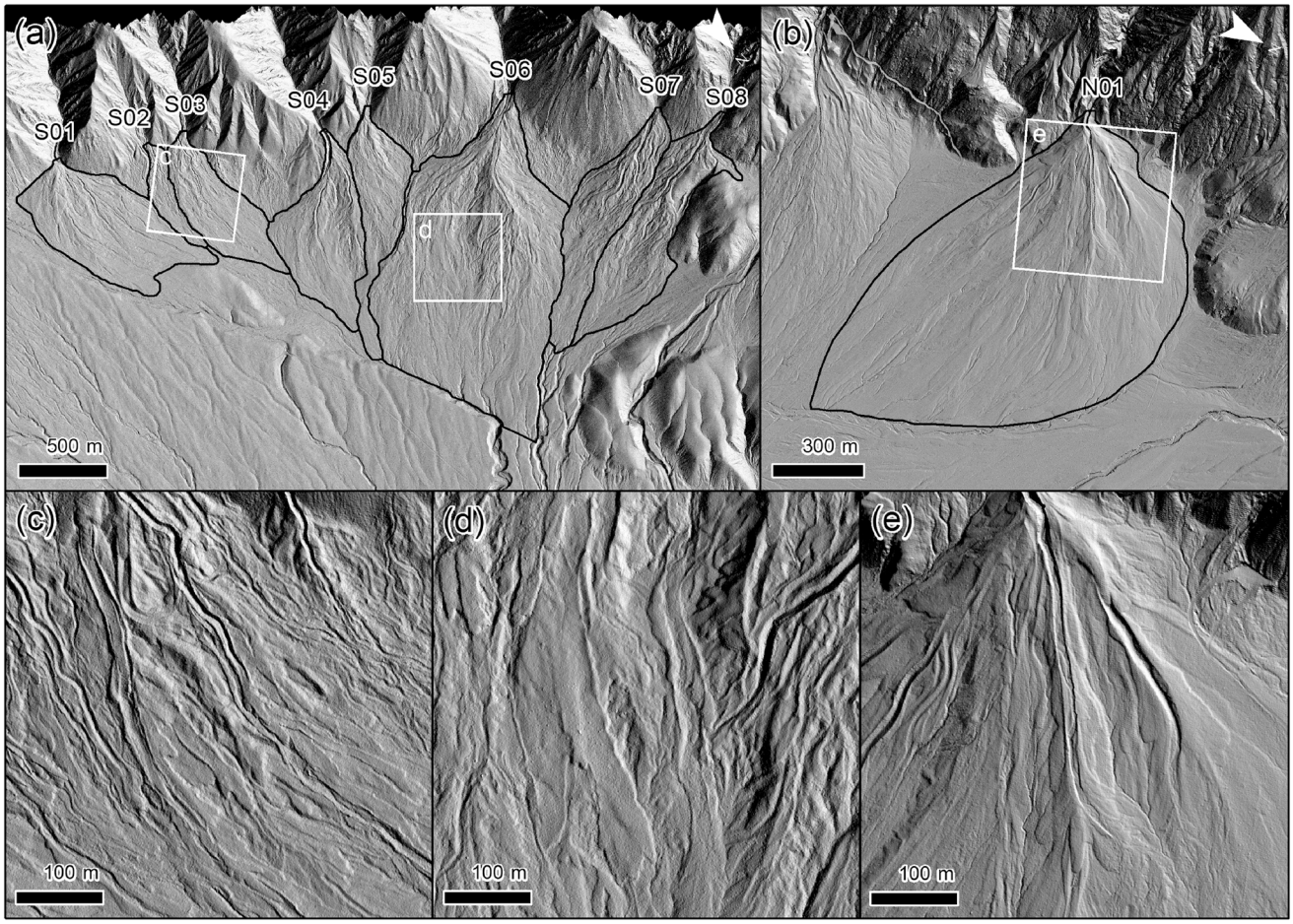

Figure 2. Hillshaded lidar elevation images of the study-area fans. (a) Fans S01–S08, on the southern margin of Saline Valley. (b) Fan N01, on the northwestern margin of Saline Valley. Lower panels show detailed views of debris-flow channels and lobes on (c) fans S02 and S03, (d) fan S06, and (e) fan N01. See Figure 1 for location of panels (a) and (b). Black lines in panels (a) and (b) show the approximate outlines of individual fans defined by eye.

Eight of the study fans, S01–S08, form a bajada in the southern part of the valley, while fan N01 is located in the northwestern part of the valley (Figure 2). The apices of the southern fans are located at an elevation of ~1,200 m above sea level (asl), while the apex of fan N01 has an elevation of 700 m asl (Table 1). The catchments of the fans extend up to ~1,600 m asl for the smallest systems to ~2,300 m asl for the largest catchments, spanning 400–1,200 m of relief. Catchment areas range from 0.1 to 3 km^2, and mean catchment

Table 1
Study Site Characteristics

	Fan characteristics		Catchment characteristics				
Fan	Area (km^2)	Mean slope (°)	Area (km^2)	Min. Elevation (m)	Max. Elevation (m)	Elevation range (m)	Mean slope (°)
N01	0.79	6.2	0.91	762	1754	992	29.0
S01	0.42	8.4	1.89	1208	2162	954	23.1
S02	0.07	9.8	0.15	1206	1597	391	33.7
S03	0.23	9.2	0.49	1186	1889	703	28.5
S04	0.33	7.7	2.21	1173	2214	1041	24.4
S05	0.24	11.0	0.36	1171	1813	642	30.1
S06	1.32	7.4	2.92	1168	2336	1168	24.5
S07	0.31	9.4	0.44	1221	1817	596	29.9
S08	0.38	9.6	0.74	1215	1998	783	22.9

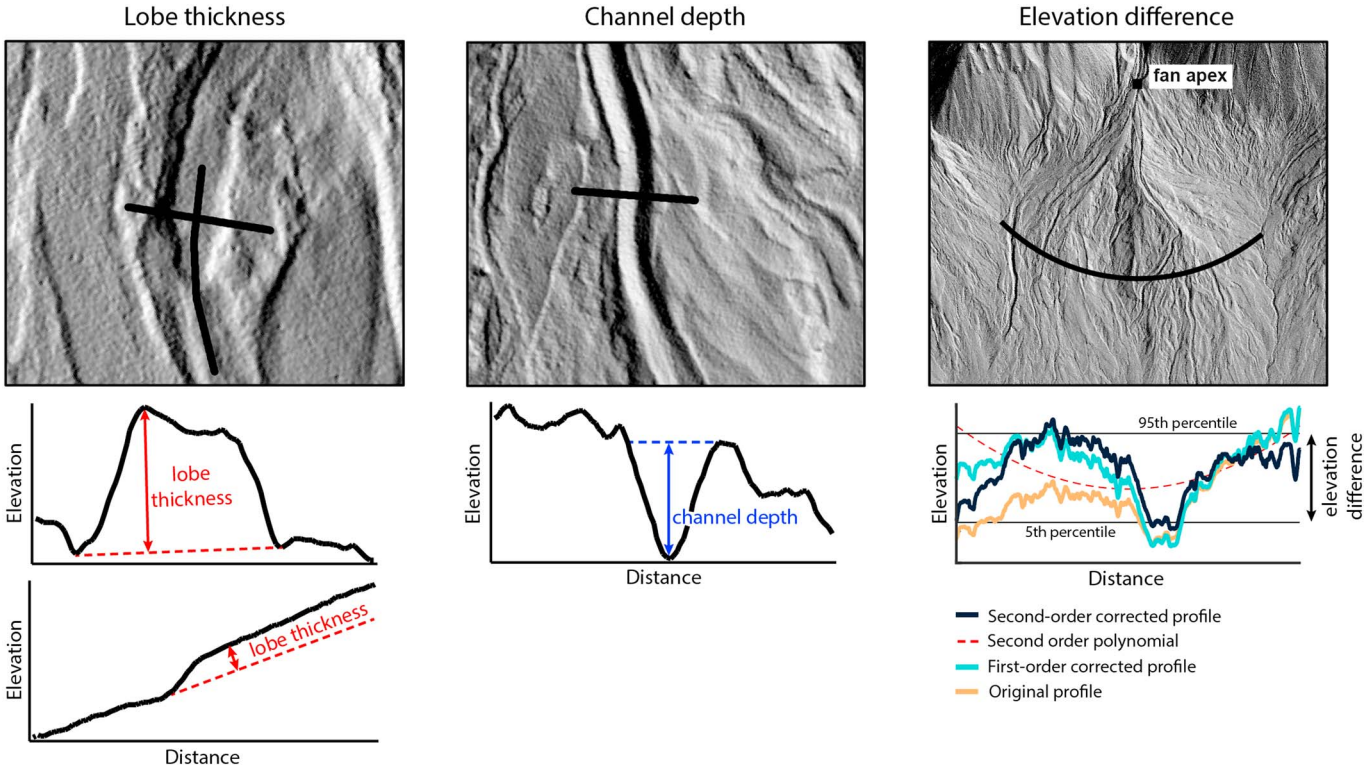

Figure 3. Definition of measurement techniques for lobe thickness, channel depth, and channel-bed superelevation.

slopes are 23–30°. Fan areas are between 0.07 and 1.3 km^2. The southern fans have slightly higher mean slopes than the northern fan N01: 7.5–11° and 6°, respectively.

Fans S01–S08 are fed by catchments in the Nelson Range that are entirely underlain by the Jurassic Hunter Mountain quartz monzonite batholith (Burchfiel et al., 1987; Chen & Moore, 1982; Hall & McKevitt, 1962; McAllister, 1956; Oswald & Wesnousky, 2002). The northern fan N01 is fed by a catchment in the eastern Inyo Mountains that is mostly underlain by Paleozoic metasedimentary rock (marble, quartzite, and chert), while some quartz monzonite and shale are present near the top of the catchment (Conrad & McKee, 1985; Ross, 1967). Vegetation is sparse in the study area, and sediment appears to be supplied to the catchments by both shallow and bedrock landsliding as well as rockfall from exposed bedrock faces.

The fans have developed in response to slip and accommodation generation on the Hunter Mountain and Saline Valley fault zones (Oswald & Wesnousky, 2002). The slip rate on the Saline Valley vault zone since 15 ka has been estimated at 3.3–4.0 mm/year (Oswald & Wesnousky, 2002), while the present-day slip rate on the Hunter Mountain fault zone has been estimated at 5 mm/year (Gourmelen et al., 2011).

2.2. Climatic Setting

Present-day mean annual temperature is ~10 °C in the catchment headwaters and ~18 °C on the fan surfaces (PRISM, 2004). Saline Valley is located in the rain shadow of the Sierra Nevada and Inyo Mountain ranges to the west, although the majority of precipitation in the study area originates from Pacific sources to the west (Antinao & McDonald, 2013; D'Arcy et al., 2017). Mean annual precipitation is 200 mm/year near the catchment crest and 120–140 mm/year on the fan surfaces (PRISM, 2004). Most precipitation falls in the winter period, although precipitation intensities may be higher in summer (Beaty, 1963). Debris-flow activity in the study area appears to be mostly associated with high-intensity summer thunderstorms (Beaty, 1963; Blair & McPherson, 1998; DeGraff et al., 2011; Hubert & Filipov, 1989; Miller et al., 2010). Historical records from nearby Owens Valley reveal that approximately 75% of the recorded floods have occurred during the summer months (Beaty, 1963). Given their proximity, we assume that climatic conditions are similar for the study fans in the southern and northwestern parts of Saline Valley and that this similarity has persisted over time.

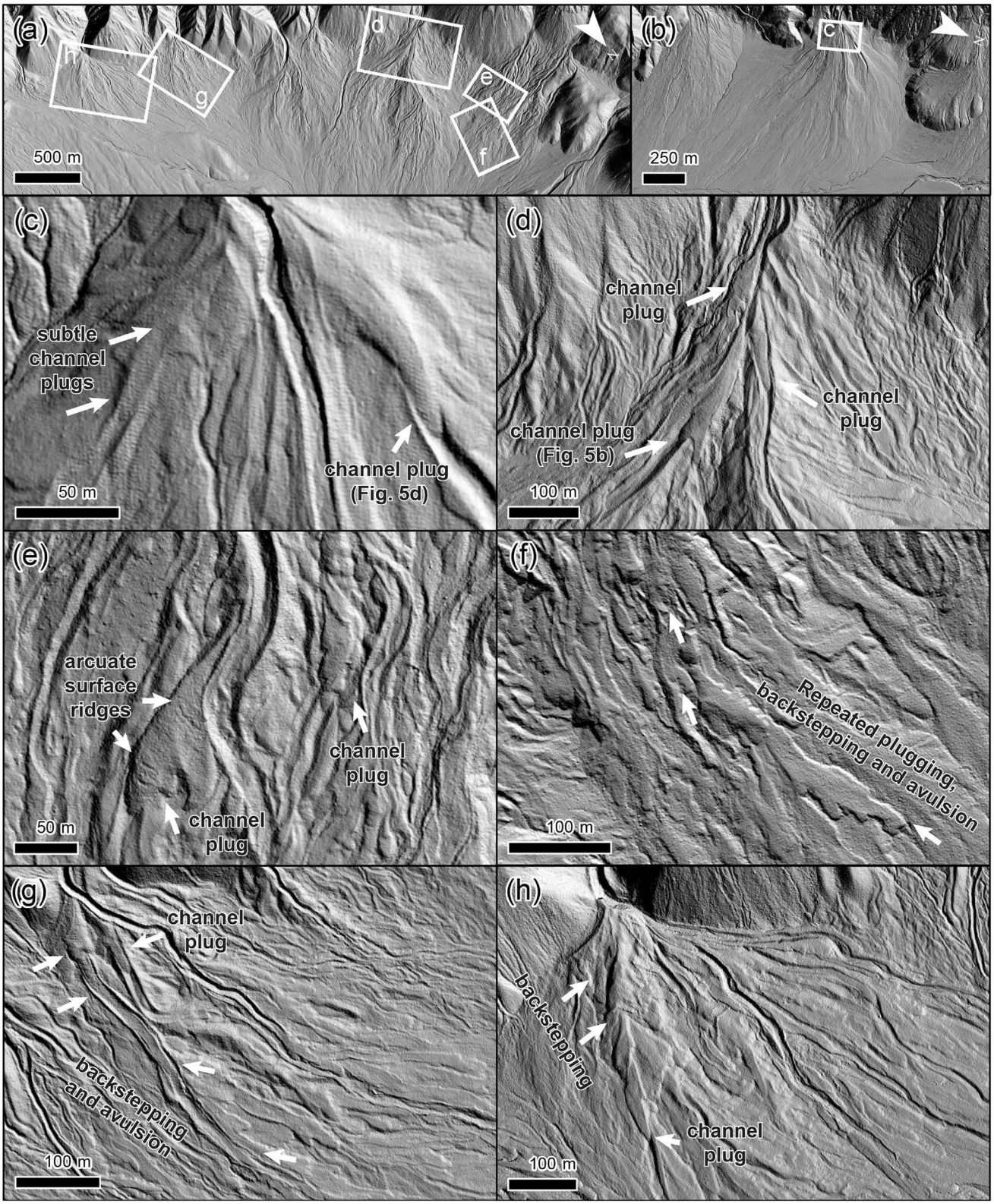

Figure 4. Fan-surface morphology and examples of avulsion sites. (a) Locations for the images on the southern fans. (b) Location for the image on the northern fan N01. (c) Channel plugs on fan N01. (d) Channel plugs on fan S06. (e) Channel plugs on fan S07. (f) Two inferred sequences of plugging, backstepping, and avulsion within the active channel of fan S08. Arrows show backstepping lobes. (g) Backstepping toward the apex in a channel on fan S03, finally resulting in avulsion. Arrows show backstepping lobes. (h) Channel plugging, backstepping, and avulsion on fan S01. Arrows show backstepping lobes.

Figure 5. Examples of debris-flow lobe deposits plugging channels. (a–c) Fan S06. (d–f) Fan N01. See Figure 4 for locations of panels (b) and (d). Geologist for scale (circled in panel e) is 1.9 m tall.

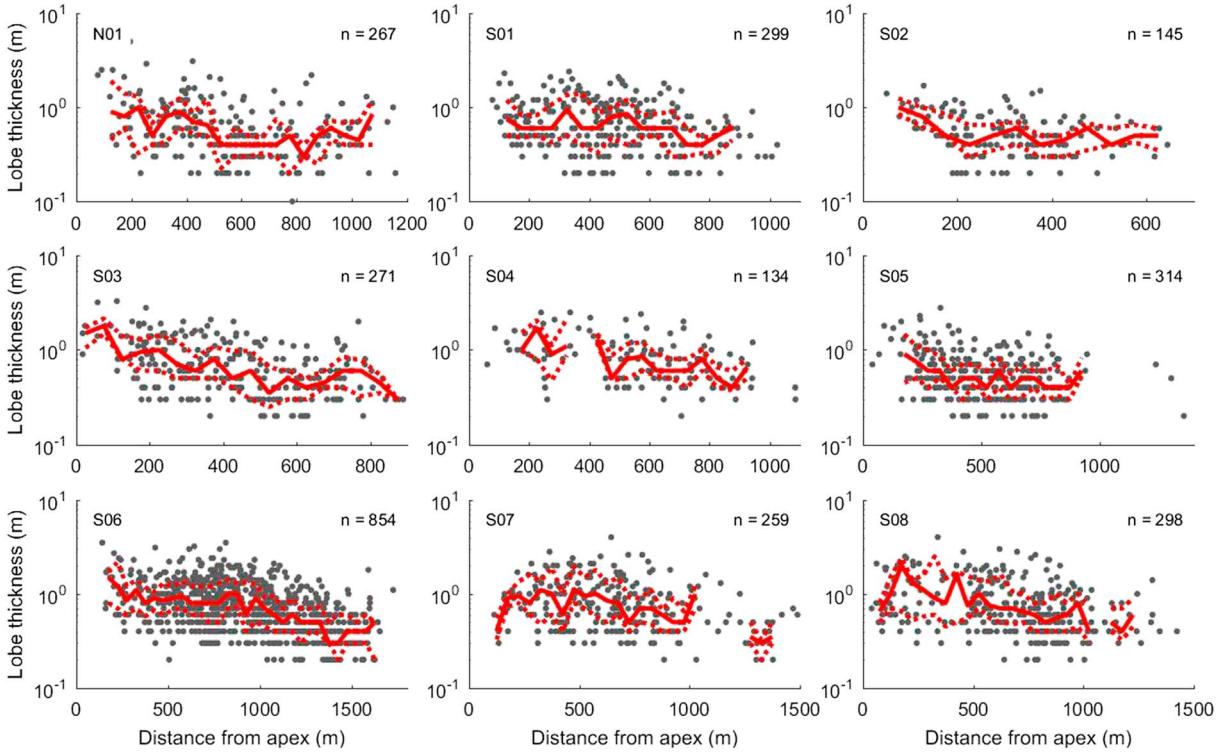

Figure 6. Relationships between debris-flow lobe thickness and distance from fan apex for each of the study-area fans. The solid red line indicates the median value per 50-m distance bin, and dashed lines indicate the 25th and 75th percentiles per 50-m radial distance bin. No percentile lines are plotted for bins with less than three data points. Note changes in horizontal scales between panels, the general downfan decrease in lobe thickness on all fans, and the high degree of variability at any downfan distance.

By studying multiple fans with similar climatic settings, including some (fans S01–S08) that share a common bedrock lithology, we can largely eliminate autogenic and allogenic variability and determine the underpinning factors that control avulsion location. Comparison between fans S01–S08 and the northern fan N01 provides a partial look at the potential role of lithology in setting avulsion location and mechanism.

3. Materials and Methods

3.1. Topographic Analyses

We measured fan-surface topography, including lobe and channel dimensions and channel-bed superelevations, from a lidar topography data set with 0.5-m spatial resolution. The data were collected in April 2007 by the National Center for Airborne Laser Mapping (NCALM; available for download at www.opentopography.org).

Debris-flow lobes were manually identified and mapped using hillshade, curvature, and local slope maps (e.g., Roering et al., 2013; Staley et al., 2006). Debris-flow lobe thickness, width, width/depth ratio, and cross-sectional area were manually measured from the lidar topography, with a minimum resolved thickness of 0.1 m and minimum resolved width of 2 m. Lobe thickness was determined as the maximum thickness extracted from an elevation cross-profile and/or long profile, assuming a planar deposit base (Figure 3). Lobe width was determined as the maximum width of the lobe deposit along its mappable length. Lobe width/depth ratio was calculated by dividing the measured lobe width by the measured lobe thickness. Cross-sectional area was calculated by assuming that the debris-flow lobes were trapezoidal in cross section, with an area of 0.75 × lobe width × lobe thickness (e.g., De Haas, Hauber, et al., 2015). Lobe width can be accurately measured, but our assumption of a planar bed underneath the debris-flow lobe deposit will cause underestimation or overestimation of the true thickness in the likely event of a nonplanar deposit base. The errors introduced were then subsequently propagated into the calculations of width/depth ratio and cross-sectional area. The largest error in lobe cross-sectional area was, however, likely associated with any deviations from a trapezoidal cross-sectional shape. The two extreme end-members of cross-sectional shape would be a triangle and rectangle, yielding a conservative accuracy of ±25%. In reality, the errors are

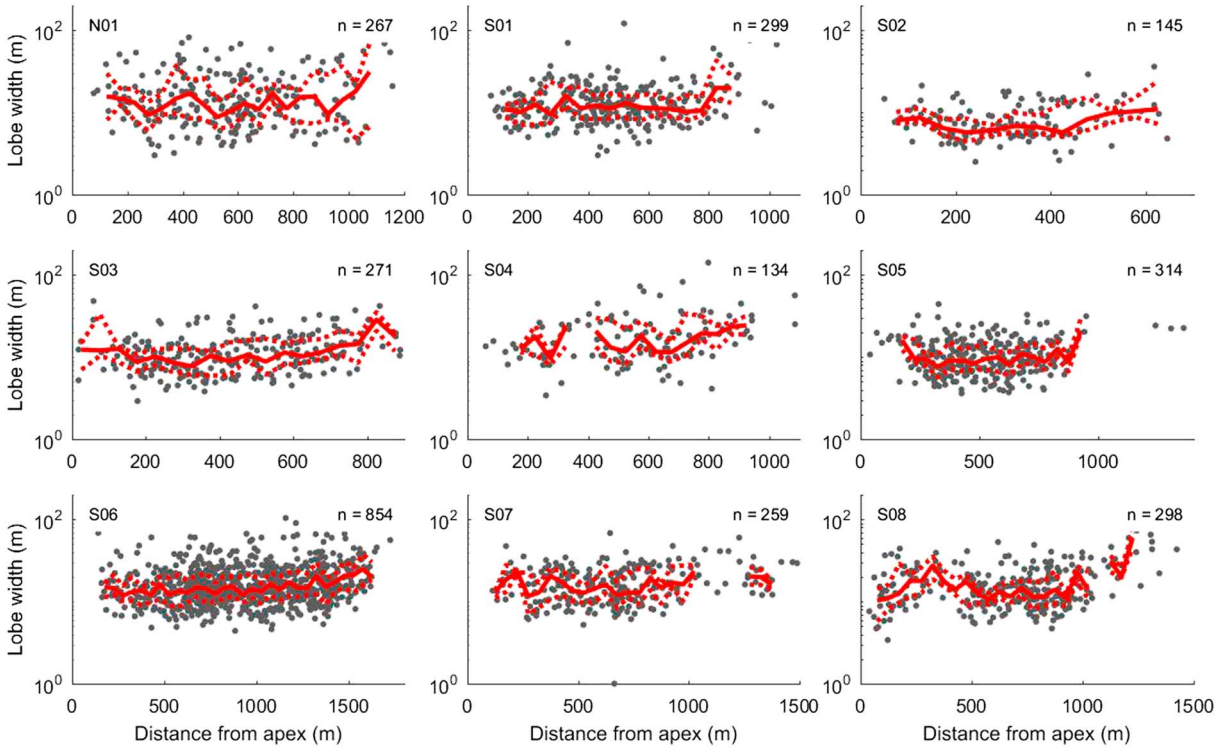

Figure 7. Relationships between debris-flow lobe width and distance from fan apex. The solid red line indicates the median value per 50-m radial distance bin, and dashed lines indicate 25th and 75th percentiles per 50-m distance bin. No percentile lines are plotted for bins with less than three data points. Note changes in horizontal scales between panels, the general downfan increase in lobe width on all fans, and the high degree of variability at any downfan distance.

likely smaller and are much smaller than the variability in lobe dimensions observed on the fans (see section 4.2). Therefore, errors in the measurement of lobe dimensions do not influence any of the trends or results demonstrated here. As such, we do not present error bars on the data. Finally, we approximated the runout distance of each flow as the shortest distance between the fan apex and the terminal position of debris-flow lobes. This straight-line distance will underestimate the true flow path length, but we can only trace the full flow path of the most recent flows as a result of overprinting of older flow paths by more recent events. To enable comparison of runout distributions on fans with different areas and numbers of flows, we then normalized the number of terminal lobe positions by the available fan area in concentric distance bins of 50-m width, centered on the fan apex. Exposed plug lengths vary from a few meters to a few hundred meters at maximum.

The sequence of activity in different channels, and associated avulsion locations, were identified and mapped from cross-cutting relationships. Channel depths were determined by extracting elevation profiles perpendicular to the channel midline at 1-m intervals in a downstream direction. Channel depth was then defined as the elevation difference between the lowest point in the channel thalweg and the highest point on the lower of the two banks (Figure 3).

To determine how channel-bed superelevation varies across each fan surface, concentric semicircular elevation profiles centered on the fan apex were extracted in a downfan direction at a fixed radial distance interval of 25 m (Figure 3). First- and second-order polynomials were successively fitted and extracted from each elevation profile to correct for lateral skewness and fan convexity, respectively (Figure 3). We did this because avulsions will generally only be able to occupy the nearest local low from the avulsion point rather than the absolute low on the entire fan surface. By correcting for lateral skewness and fan convexity, we could quantify the local fan-surface relief, which is a direct measure of superelevation, rather than the absolute relief difference. We then defined the elevation difference at a given radial distance from the fan apex as the 95th minus the 5th percentile elevations within each elevation profile, to filter out the extreme low and high values. Channel superelevation was then calculated by dividing the elevation difference by the median channel

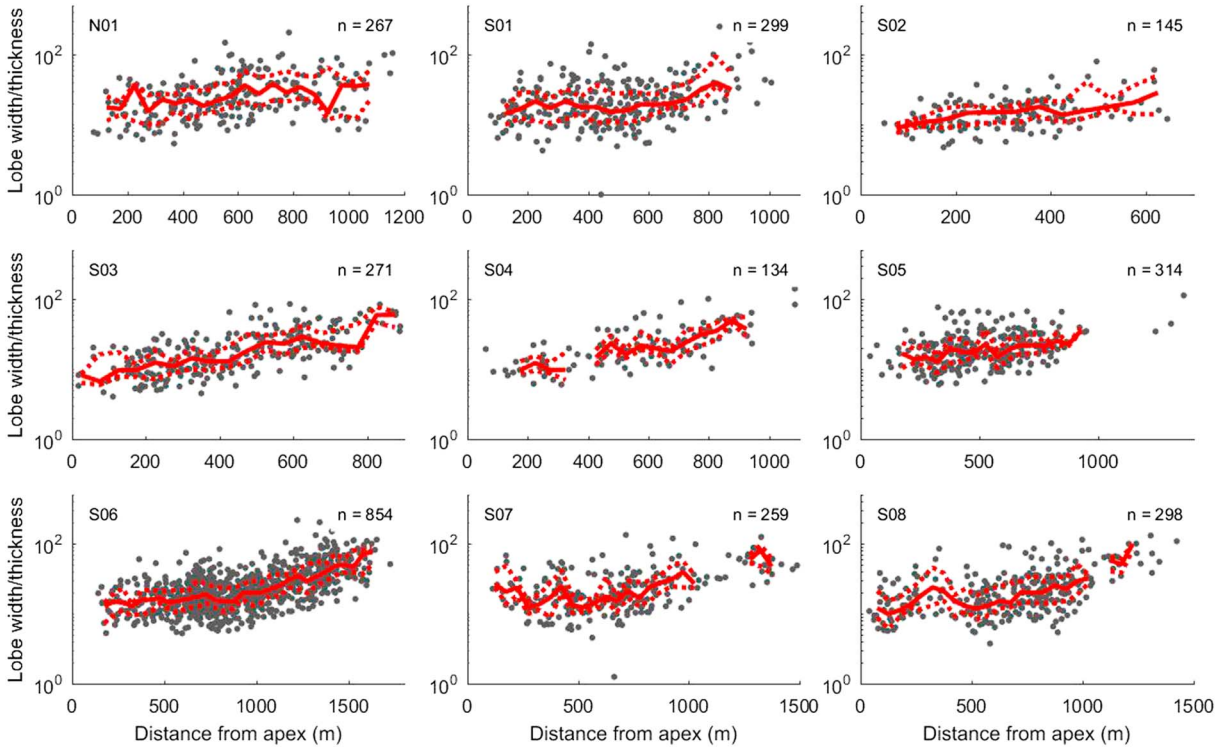

Figure 8. Relationships between debris-flow lobe width/thickness ratio and distance from fan apex. The solid red line indicates the median value per 50-m distance bin, and dashed lines indicate 25th and 75th percentiles per 50-m radial distance bin. No percentile lines are plotted for bins with less than three data points. Note changes in horizontal scales between panels and the general downfan increase in width/thickness ratio.

depth within the 25-m radial distance bin centered on each profile. This yields an estimate of superelevation as a multiple of the median channel depth in that bin.

3.2. Grain-Size Measurements

We determined approximate grain-size distributions of clasts at the frontal margins of 115 debris-flow lobes on one of the fans, S06, using close-range photosieving (e.g., Carbonneau et al., 2004; De Haas et al., 2014). This method does not yield the full grain-size distribution, including matrix material, but provides a rapid and approximate indication of the distribution of coarse (medium sand-sized and greater) clasts that can be compared across the fan surface. For each of the 115 debris-flow lobes, two plan-view images were taken of the frontal margins with a commercial digital camera. For each image, roughly covering 3 m × 2 m, a ruler was placed within the frame to establish scale. The apparent long and intermediate axes (a and b, respectively) of 25 clasts were measured at random positions on the image. The measurements from the two images were subsequently combined, yielding grain-size distributions of 50 grains for each debris-flow lobe. We acknowledge that the limited sample size of 50 particles introduces substantial uncertainty in the grain-size statistics (Rice & Church, 1996). We chose this number to allow rapid comparison across all of the lobes and because of the limited number of large clasts in the lobes, which means that further grain-size measurements would add to the proportion of smaller grain sizes but would not change the count of the coarsest fraction. Particles with b axes smaller than 3 pixels were below the resolution of the method and were assigned a default size of 3 pixels (~0.3 mm). Particle b axes were used to calculate a probability density function by number, using an arithmetic grain-size distribution (e.g., Blott & Pye, 2001).

4. Results

4.1. General Fan Morphology

Fan surfaces in Saline Valley are composed of well-defined channels, debris-flow lobes, and levées (Figures 2 and 4). Lobe deposits are the most abundant morphological feature on the surfaces. There is very limited evidence for stream-flow activity on the fans; where evident, it is limited to minor reorganization and sediment sorting in channel thalwegs. Meter-scale boulders are abundant on the southern fans, S01–S08, in both

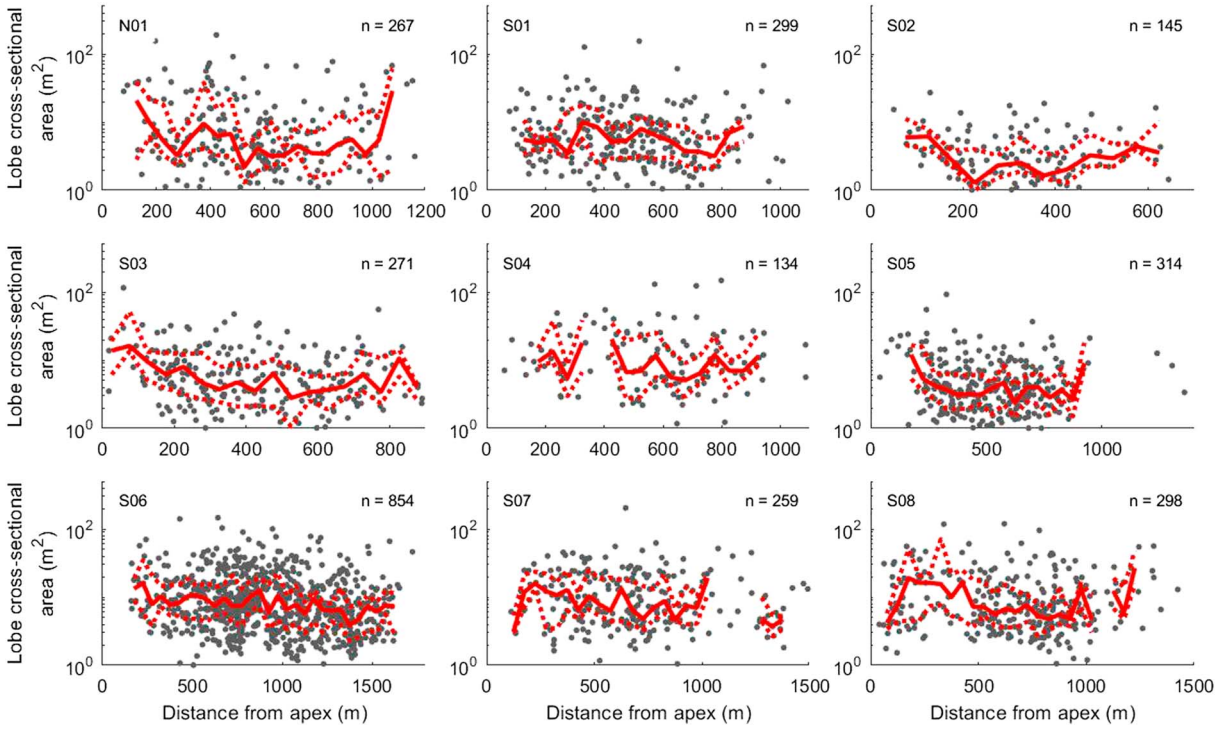

Figure 9. Relationships between debris-flow lobe cross-sectional area and distance from fan apex. The solid red line indicates the median value per 50-m radial distance bin, and dashed lines indicate 25th and 75th percentiles per 50-m distance bin. No percentile lines are plotted for bins with less than three data points. Note changes in horizontal scales between panels and lack of a consistent downfan trend in cross-sectional area.

lobe and levée deposits across the fan surfaces, while the deposits on the northern fan, N01, are generally finer, with very few meter-scale boulders.

The downfan toes of debris-flow lobes are generally coarser grained than the rest of the deposit (Figure 5). The maximum grain size of lobe deposits differs between lobes, ranging in diameter from a few decimeters to over a meter, and the same holds for levée deposits. The lobes are mostly matrix supported, although some lobes have an open-work clast-supported texture at their toes.

Lateral boundaries of lobe and levee deposits are sharp and well-defined across all fan surfaces, and primary flow features such as flow margins, lateral levées, and coarse-grained snouts can still be recognized. There is very little evidence for secondary reworking from fluvial or eolian processes on the fan surfaces. This suggests that the debris-flow lobe and channel dimensions that can be observed at present are very similar to the dimensions at the time of deposition.

4.2. Spatial Trends in Debris-Flow Lobe Dimensions

Debris-flow lobe thickness generally decreases from fan apex to toe on all of the studied fans (Figure 6), and on most of the fans the decrease is largest close to the fan apex. There is considerable variability in lobe thickness at all distances from the fan apex; lobes typically range from a few decimeters up to a few meters in thickness at a given radial distance. The median thickness of the lobes differs slightly between the fans, but on average median lobe thickness decreases from ~1 m near the fan apex to ~0.5 m near the fan toe, while maximum lobe thickness generally decreases from 3–5 m near the fan apex to ~1 m near the fan toe.

In general, there is a slight increase in debris-flow lobe width from fan apex to fan toe (Figure 7). Variability in lobe width is large at all distances from the fan apex, however, and lobe width can range from a few meters to a few tens of meters at all distances from the fan apex. Absolute lobe width slightly differs between fans, but median width generally increases from 10–15 m near the fan apex to 15–25 m near the fan toe. Similarly, maximum widths are generally greater near the fan toe than near the fan apex.

As a result of these trends, the debris-flow lobe width/thickness ratio increases from fan apex to fan toe for all fans (Figure 8). Variability is large at all distances from the fan apex, however, with lobe width/thickness ratios potentially ranging from <5 to >100. Near the fan apex the median lobe width/thickness ratio is gen-

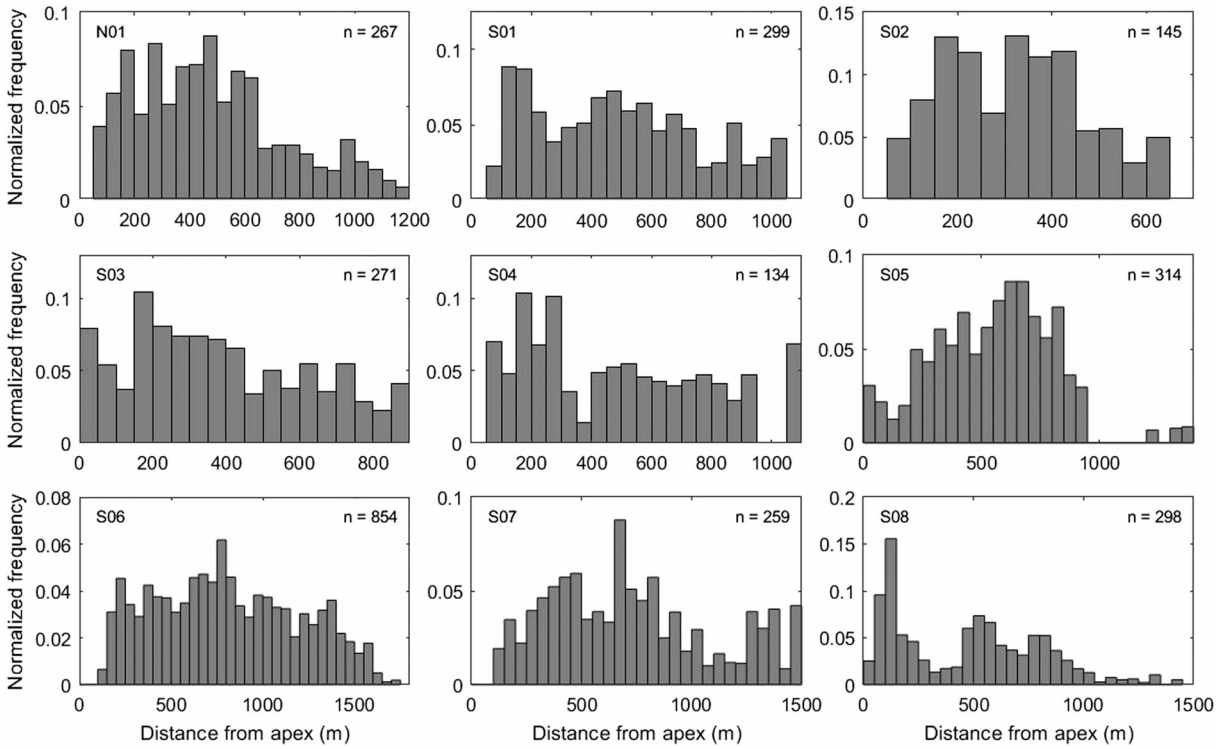

Figure 10. Histograms of the distance between the fan apex and debris-flow lobe termination points, as a proxy for runout distance, for 50-m distance bins, normalized by available fan area per bin. There is a slight preference for lobe deposition on the upper half of the fan surfaces, especially on fans N01 and S08, but this is not universal across all fans.

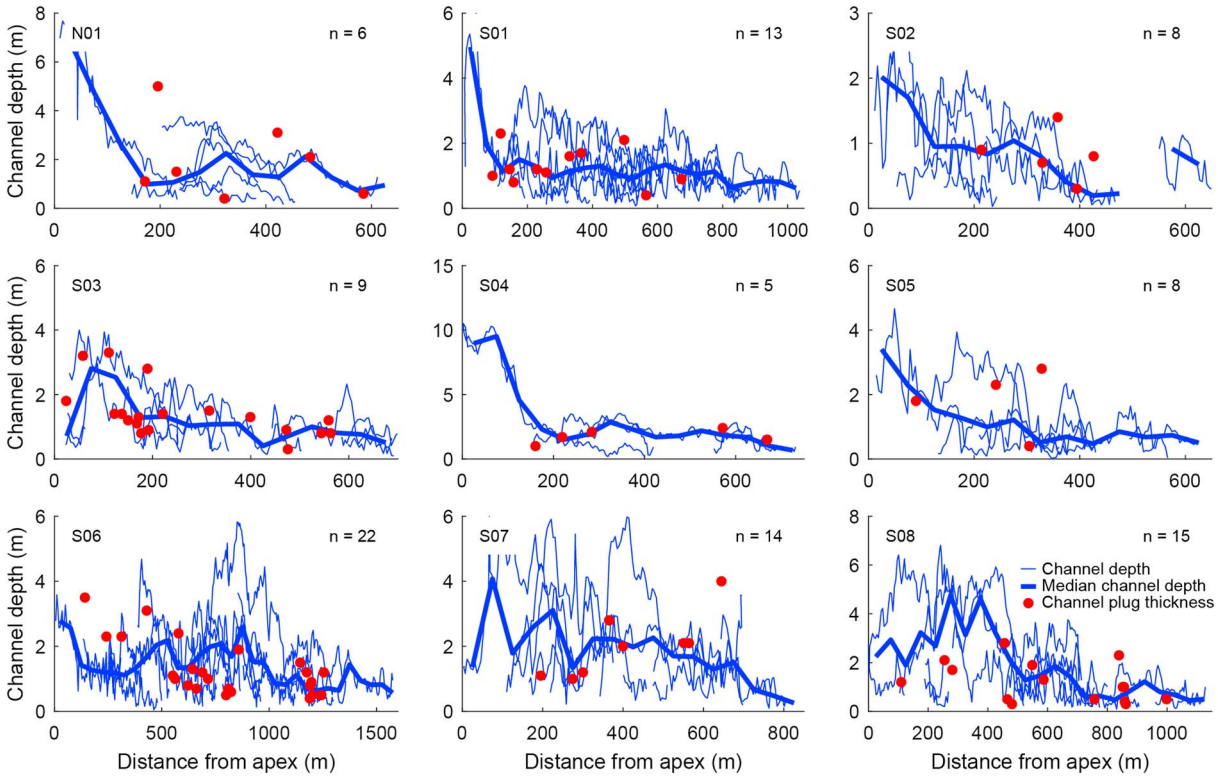

Figure 11. Variation of channel depth with distance from fan apex. Thin blue lines indicate the depths of individual channels. The thick blue line indicates the median channel depth per 50-m radial distance bin on each fan. Dots show the locations and thicknesses of channel plugs associated with avulsion locations on each fan (see, e.g, Figures 4 and 5). Note that plug thicknesses are roughly evenly distributed around the median channel depth on all fans.

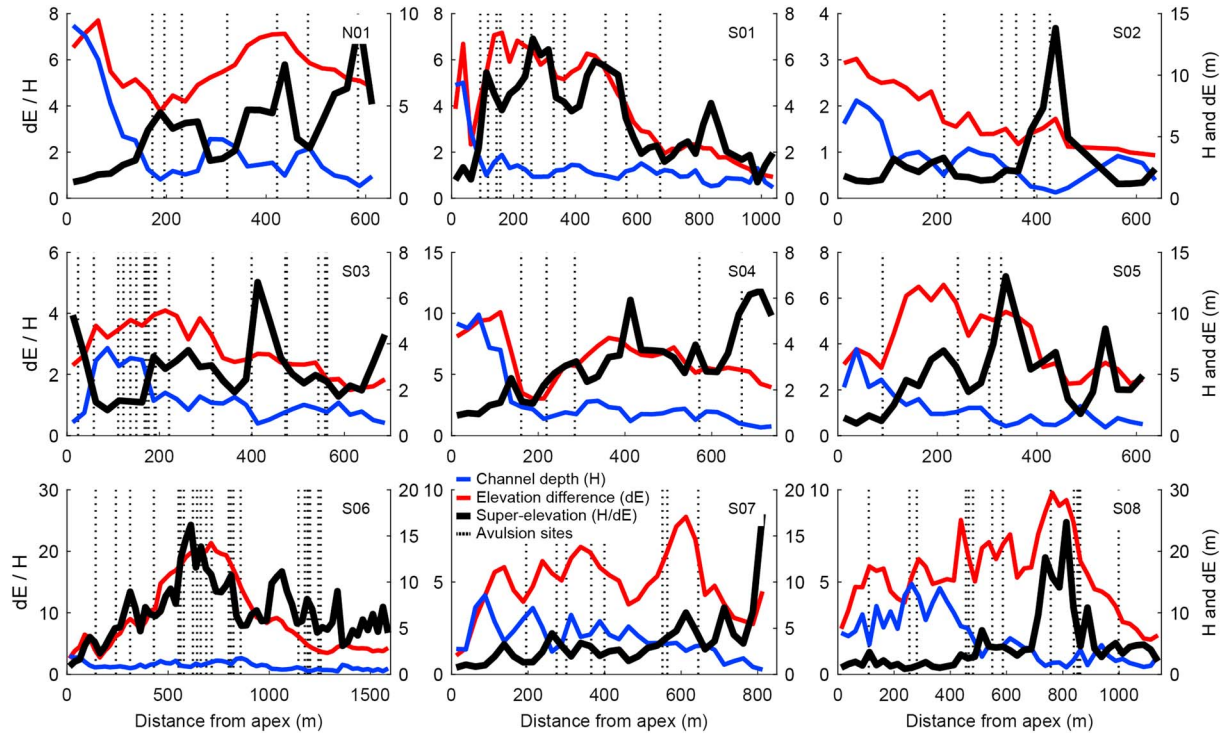

Figure 12. Median channel depth (H, blue lines), elevation difference (dE, red lines), and channel-bed superelevation (dE/H, thick black lines) versus distance from fan apex for 25-m radial distance bins. The radial distances of avulsion sites (channel-plug locations) are indicated by vertical dashed lines (also see Figure 11 for channel-plug locations). Note the lack of a clear correspondence between avulsion sites and high superelevation values.

erally on the order of 10–20 and increases up to 50–100 near the fan toe. The maximum lobe width/thickness ratios follow a similar increasing trend from fan apex to fan toe. Thus, debris-flow lobes on the studied fans become thinner and wider with increasing distance from the fan apex (Figures 6 and 7).

The cross-sectional area of the debris-flow lobes, however, remains nearly uniform or decreases only slightly from fan apex to fan toe (Figure 9). On two of the studied fans, S03 and S06, the median cross-sectional area of the debris-flow lobes decreases slightly from approximately 15 m^2 near the fan apex to 10 m^2 near the fan toe. On the other fans the cross-sectional area of the debris-flow lobes remains approximately uniform with distance from the fan apex, at around 5–15 m^2 depending on the fan system. The maximum cross-sectional area of the lobes on the fans ranges from ~30 m^2 on fan S02 to >100 m^2 on fan S06.

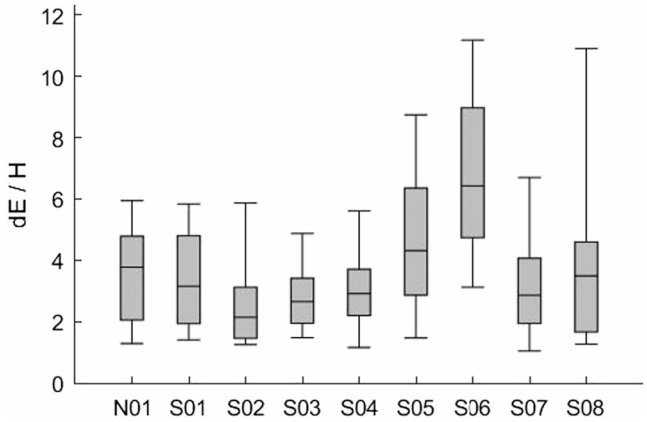

Figure 13. Boxplots of channel-bed superelevation (dE/H) for each of the studied fans. Boxes indicate quartiles, horizontal lines indicate the median, and whiskers indicate the 10th and 90th percentiles.

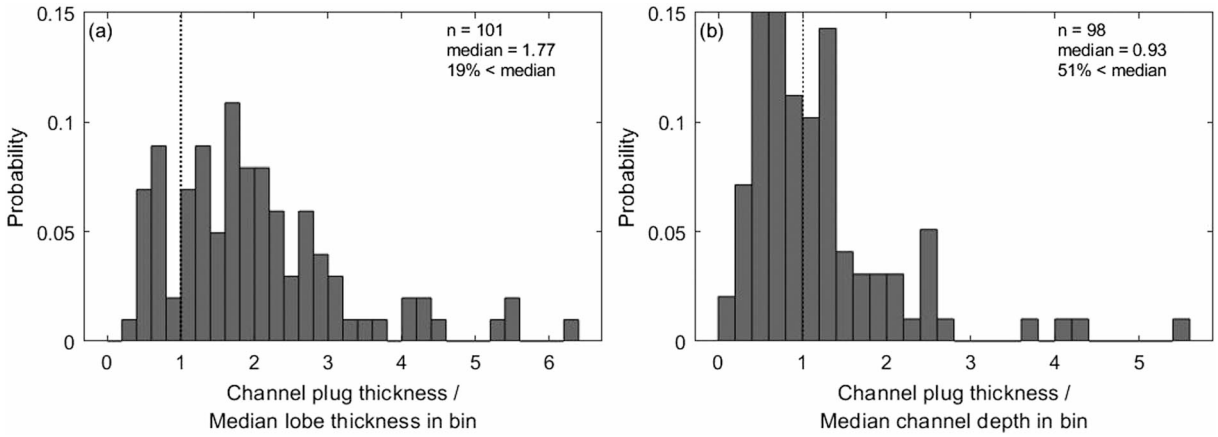

Figure 14. Channel-plug characteristics. (a) Histogram of channel-plug thickness divided by the median lobe thickness in the same 50-m radial distance bin. A total of 81% of the debris-flow lobes that plug a channel and cause avulsion are thicker than the median thickness within that distance bin. (b) Histogram of channel-plug thickness divided by the median channel depth in the same distance bin. A total of 49% of the debris-flow lobes that plug a channel and cause avulsion have a thickness larger than the median channel depth.

4.3. Runout Distribution

Histograms of the terminal positions of debris-flow lobes, normalized by available fan area per 50-m radial distance bin, do not show a consistent pattern between fans. Debris-flow runout distances are roughly uniformly distributed, with a slight preference for terminal lobe deposition on the upper half of the fan surface on most but not all fans (Figure 10). This downfan decrease in terminal positions, most notable on fans N01 and S08, is probably the result of the increasing width of the distal debris-flow lobes. There are several hot spots where terminal lobes are relatively abundant, for example, around 650 m from the apex on fan S05, around 700 m from the apex on fan S07, and around 150 m from the fan apex on fan S08.

4.4. Longitudinal Trends in Channel Depth

Median channel depth decreases with distance from the fan apex (Figure 11). Channel depths near the apex can be up to 10 m as a result of fan-head incision, such as on fans N01, S01, and S04. These incised reaches typically do not extend beyond 200 m downfan of the apex. Further downfan, the median channel depth is generally 1–2 m. At all distances from the fan apex, however, channel depths can vary from a few decimeters to a few meters. Moreover, locally very deep channels can be found, such as around a distance of 200 m from the apex on fan S05, 800 m from the apex on fan S06, and 400 m from the apex on fan S07. The high variability in channel depth occurs both along individual channels and between different channels on the same fan surface.

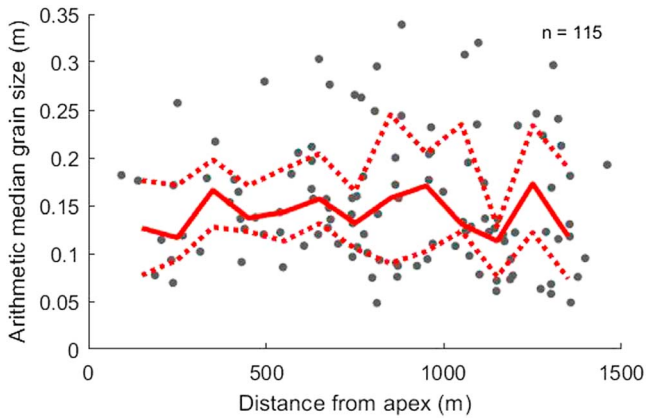

Figure 15. Relationship between debris-flow lobe arithmetic median grain size and distance from fan apex for fan S06. The solid red line indicates the median value per 100-m radial distance bin, and the dashed lines indicate the 25th and 75th percentiles per 100-m radial distance bin. No percentile lines are plotted for bins with less than three data points. Note that there is no clear relationship between distance from the apex and median grain size.

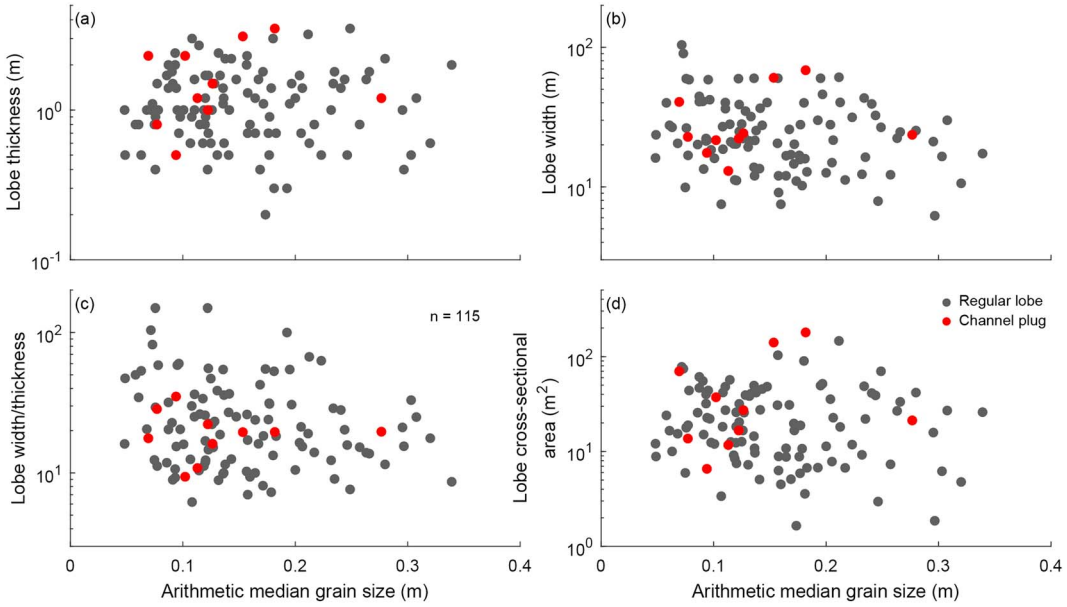

Figure 16. Relationships between debris-flow lobe arithmetic median grain size and different measures of lobe dimensions on fan S06: (a) lobe thickness; (b) lobe width; (c) lobe width/thickness ratio; (d) lobe cross-sectional area. Red symbols indicate lobes that form channel plugs associated with an avulsion. Note logarithmic *y* axes, and the lack of clear-cut trends in any of the panels.

4.5. Channel-Bed Superelevation

Channel-bed superelevation varies strongly both between fans and with radial distance from the apex on an individual fan (Figure 12). Superelevation values can be as high as >20 channel depths but are typically 2–5 channel depths (Figure 13). Fan S06 has particularly high superelevation values, with quartiles ranging from 4 to 9 channel depths and a median of ~7, as a result of very persistent deposition along the two most recently active channels. Channels can thus be strongly superelevated on the studied debris-flow fans, and the range of potential channel-bed superelevations is large.

4.6. Avulsion-Site Characteristics

Debris-flow lobes are present at the far upstream end of the majority of abandoned channels (Figures 4 and 5). These lobes have formed channel plugs composed of either a single lobe or a set of multiple backstepping lobes and mark the cessation of activity in the channel and an avulsion to a new channel location. In total, we identify 101 plugs across all of the fan surfaces.

Plugs are generally most abundant near the fan apex but can be present virtually anywhere on the fan surfaces (Figure 11). Plugs also tend to be relatively thick; their thickness exceeds the median size of the lobes in the same 50-m-wide radial distance bins for 81% of the 101 observed plugs (Figure 14a). The median ratio between channel-plug thickness and median lobe thickness is 1.8. Most of the channel plugs have a thickness that exceeds the median lobe thickness by 1–3 times, although some channel plugs exceed the median lobe thickness by a factor of >5.

Locally, channel-plug thickness is approximately similar to channel depth. Channel-plug thickness can be compared to median channel depth for 98 of the 101 observed plugs and exceeds the median channel depth in 49% of those cases (Figure 14b). The median ratio of channel-plug thickness to median channel depth is 0.93, although this ratio can vary from 0.2 to >5. The observed variability in this ratio is the result of the large variability of channel depth at any distance from the fan apex.

There is no consistent relationship between the pattern of channel-bed superelevation and the locations of avulsion sites (Figure 12). For example, avulsion sites on fan S03 are relatively abundant 100–200 m downstream of the apex where superelevation is particularly low. They are also abundant 600–750 m downstream of the apex of fan S06, where superelevation is high.

4.7. Grain Size

There is no relationship between distance from the apex of fan S06 and arithmetic median grain size (of particles 0.3-mm diameter and larger) on the 115 debris-flow lobe fronts that were measured (Figure 15). Similarly, we find no trends between any other grain-size percentiles and distance from the apex. Debris-flow lobe thickness, width, width/depth, and cross-sectional area are unrelated to the arithmetic median grain size of the studied debris-flow lobe fronts (Figure 16), and debris-flow dimensions are similarly unrelated to any other grain-size percentiles. In addition, the grain-size distribution of channel plugs identified on fan S06 does not differ from the grain-size distribution of regular debris-flow lobes that do not form plugs. These results suggest that debris-flow runout distance as well as debris-flow lobe dimensions and the likelihood of plug formation on this fan are not directly related to the particle-size distributions of the flow fronts—at least not in terms of particles that are sand sized or larger.

5. Discussion

5.1. A Probabilistic Spatial Framework for Avulsion on Debris-Flow Fans

We have evaluated the roles that (1) the superelevation of an active channel above the surrounding fan surface and (2) channel-plug formation may play in causing avulsion on debris-flow fans. The former is known to be an indicator of avulsion occurrence on fluvial fan systems (e.g., Carling et al., 2016; Jerolmack & Mohrig, 2007; Mohrig et al., 2000), while the latter landforms are unique to debris-flow fans (e.g., Beaty, 1963; De Haas, Densmore, et al., 2018; Suwa & Okuda, 1983; Whipple & Dunne, 1992).

The channels on the debris-flow fans studied here are on average elevated by 2–5 channel depths above the fan surface, and median superelevation is up to ~7 channel depths on fan S06 (Figures 12 and 13). Channel-bed superelevation is generally thus larger on debris-flow fans than on fluvial fans, on which avulsion frequency roughly scales with the time required to aggrade 0.5–1 channel depth above the floodplain (e.g., Carling et al., 2016; Jerolmack & Mohrig, 2007). Deposition therefore appears to be more persistently focused along the main channel on these fans. The large superelevation values and their variability across the study-area fans along with the lack of a clear correlation with avulsion locations suggest that superelevation is unlikely to be a strong control on debris-flow avulsion, and that it cannot be used to predict the likelihood, timing, and location of avulsions.

In contrast, our data indicate that blocking of the active channel by relatively thick depositional lobes appears to be the dominant mechanism for triggering debris-flow avulsions on these fans. While channel plugging has long been recognized qualitatively as a cause for debris-flow avulsion in our study area (e.g., Whipple & Dunne, 1992), our analysis quantitatively demonstrates that ~80% of avulsion locations are associated with lobes with greater than median thickness at that location on the fan. Channel-plug thickness typically exceeds median lobe thickness by a factor of 1–3, and sometimes by a factor of >5 (Figure 14a). Perhaps not surprisingly, the typical thickness of a lobe that is associated with an avulsion is similar to the median channel depth at that location. These findings imply that the likelihood of plug formation and avulsion depend on the ratio between debris-flow lobe dimensions and channel depths across a fan surface. We find that debris-flow lobe thickness decreases, debris-flow lobe width increases, lobe width/thickness increases, and lobe cross-sectional area remains roughly constant with increasing distance from the fan apex (Figures 6–9). On average, channel depth decreases from fan apex to fan toe (Figure 11). Yet it is also important to recognize that, as a result of the large variability in potential channel depth and lobe thickness across a fan surface, avulsions may be induced at virtually any downfan location. Thus, thick lobes are not always necessary to induce avulsion, especially where a compound plug has developed by deposition in multiple flows or surges.

The observation that both lobe thickness and channel dimensions may substantially vary at a given location on the fan makes prediction of debris-flow avulsion complex. The probability of the formation of a channel plug with sufficient thickness to induce avulsion in subsequent flows is a function of the combined probability that (1) a debris-flow lobe stops at a given location and (2) has a thickness that approximately equals or exceeds the local channel depth. The probability of channel-plug formation, and thus avulsion, increases with debris-flow lobe thickness and decreases with channel depth. To evaluate the spatial constraints on these probabilities, we compare the observed channel depths with lobe thickness percentiles on our study fans (Figure 17). Channels on many of the fans, especially in the apex region, have a depth that exceeds the maximum observed lobe thickness. Avulsions in these areas are thus unlikely to occur. On the majority of

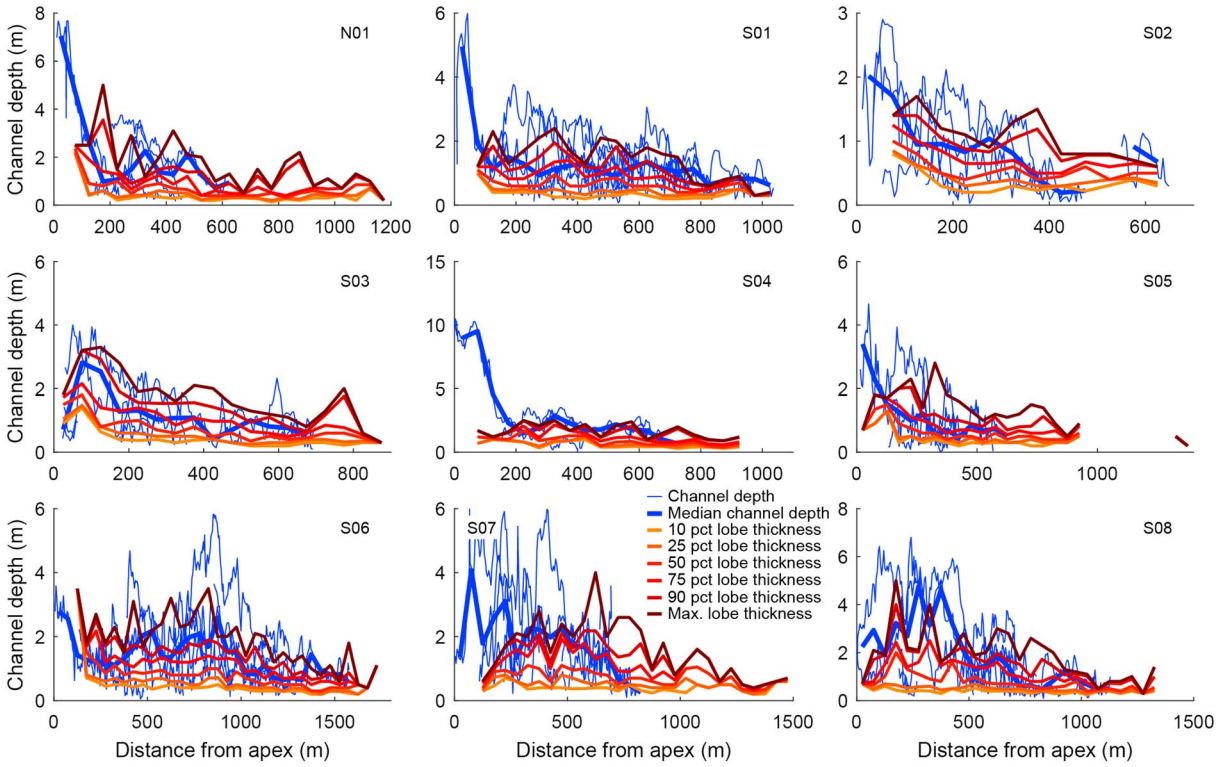

Figure 17. Channel depths (blue lines), median channel depth (heavy blue lines), and lobe thickness percentiles (warmer colors) as function of distance from fan apex. These curves indicate the probability of lobe deposition with sufficient thickness to plug the channel and cause avulsion at any distance from the fan apex.

the fans, median channel depth roughly corresponds to the 50th to 75th percentile lobe thickness, illustrating that in many areas there is a ~25–50% probability that a single debris-flow lobe has sufficient thickness to plug a channel and potentially force avulsion. The smallest measured channel depths often roughly correspond with the 10th to 25th percentile lobe thickness for most fans, implying that a lobe stopping in a region with small channel depth has a 75–90% chance to have sufficient thickness to force avulsion. Apart from deeply incised areas near the fan apices, lobe thickness percentile curves roughly have the same shape and decrease at similar rates with distance from the apex, as channel depth. This implies that debris-flow lobes generally have a similar probability to successfully plug a channel at all radial distances, which may explain our observation that avulsions are possible at any radial position.

The probability that an in-channel debris-flow lobe is sufficiently thick to cause avulsion is thus relatively large. However, for avulsion to occur, a debris-flow lobe has to deposit within a channel. Debris-flow lobes on all study-area fans are roughly uniformly distributed over the fan surface when normalized by fan-surface area (Figure 10). Because the available fan-surface area increases with distance from the apex, the absolute probability of debris-flow deposition is smaller closer to the apex. In addition, debris flows on the proximal domains of a fan are often conveyed through a channel. As long as a debris flow remains confined within a channel, its momentum remains focused and motion is therefore more likely to be sustained (e.g., Whipple & Dunne, 1992; Fannin & Wise, 2001). Debris flows therefore commonly traverse the channelized proximal parts of the fan to deposit on the more distal parts of the fan where the channels are shallower, allowing the flows to spread and lose momentum (Blair & McPherson, 1998; De Haas et al., 2016). Therefore, we infer that the relatively small chance of in-channel deposition may be one of the main limiting factors for channel-plug formation, as once deposited in a channel there is a reasonably high chance that the lobe deposit equals or exceeds the local channel depth.

The exact probabilities of in-channel deposition are currently unknown but would largely depend on flow mobility. Previous research has shown that flow mobility is a function of flow volume, water content, and particle-size distribution (e.g., Berti & Simoni, 2007; De Haas, Braat, et al., 2015; Griswold & Iverson, 2008; Iverson et al., 1998; Major, 1997; Rickenmann, 1999; Whipple & Dunne, 1992). Debris-flow lobe thickness

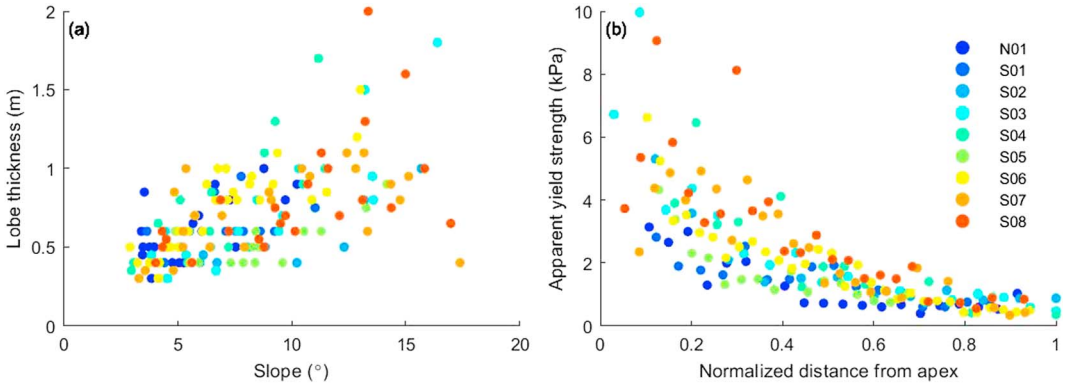

Figure 18. (a) Relationship between median fan slope and median lobe thickness per 50-m distance bin on each fan, showing overall increase in thickness at higher slopes. (b) Relationship between apparent yield strength and normalized distance from the apex per 50-m distance bin on each fan. Apparent yield strength (τ_y) is calculated as $\tau_y = \rho g h \sin\theta$.

increases with total flow volume (e.g., Berti & Simoni, 2007; De Haas, Braat, et al., 2015). Thus, the small flows that have a high probability to deposit within a channel are also less likely to be thick enough to induce avulsion, at least individually. Physical scale experiments show that debris-flow lobe thickness may increase with coarse-particle fraction (e.g., De Haas, Braat, et al., 2015), and large-volume but low-water content flows may form thick lobe deposits with restricted runout (e.g., Major, 1997). Our results, however, show that for fan S06 there is no relation between grain-size distribution at the lobe fronts, at least for grains of medium sand size and larger, and debris-flow lobe dimensions and runout (Figures 15 and 16). Although we did not measure the matrix grain-size distribution, Whipple and Dunne (1992) found no systematic relationship between matrix grain-size distribution and debris-flow mobility on a nearby debris-flow fan in Owens Valley with similar catchment lithology, which led them to identify water content as the most important control on flow mobility. Unfortunately, we have no direct observations of debris flows on our Saline Valley fans, so we are unable to constrain water contents during flow deposition.

Although our data show that the formation of channel plugs is likely to be the main avulsion control on these fans, we emphasize that without some positive channel-bed superelevation, a channel plug would not be able to induce avulsion. Once a channel is elevated above its surroundings, there must exist an alternative, topographically more favorable channel pathway. In that case, the only requirement for avulsion toward a topographic depression is that a debris flow is able to leave the active channel. Further understanding of the relative importance of these different controls on debris-flow avulsion will require comparable observations from fans in different climatic and tectonic settings.

5.2. Controls on Lobe Thickness

We have shown that the spatial distribution of lobe thicknesses across a fan surface is key to understanding the pattern of debris-flow avulsion and that lobe thickness decreases with distance from the fan apex. But what sets lobe thickness across a fan surface? We find that lobe thickness increases with local fan slope, when comparing median fan slope with median lobe thickness in 50-m radial distance bins, although considerable scatter is present (Figure 18a). Local fan slopes range between 3° and 18° and decrease from fan apex to fan toe on all studied fans.

When we combine median local fan slope (θ in degrees) and median local debris-flow lobe thickness (h in meters) for each 50-m radial distance bin from the apex, we can calculate the apparent median yield strength (τ_y in pascals) for the debris flows (e.g., Coussot et al., 1998; Johnson, 1970; Johnson & Rodine, 1984; Whipple & Dunne, 1992):

$$\tau_y = \rho g h \sin\theta \tag{1}$$

where ρ is the bulk density of the debris flow (here assumed to be 2,000 kg/m^3; e.g., McArdell et al., 2007) and g is acceleration due to gravity (9.81 m/s^2). We recognize that most natural debris flows, especially flows with accumulations of large particles near the frontal flow margins such as on our study-area fans, do not behave as Bingham plastic fluids (e.g., Iverson, 2003). Therefore, we cast this analysis in terms of bulk

apparent yield strength and interpret it as a general measure of the mobility and frictional resistance of the flows, where flows with higher apparent yield strength experience more friction and are less mobile.

Apparent yield strength typically strongly decreases in the first 200 m downstream of the fan apex, beyond which it decreases at a lower rate toward the fan toe (Figure 18b). Near the fan apex, apparent yield strength may be as large as 5–10 kPa, while it decreases to values of ~0.5 kPa near the fan toe. While the general trend of apparent yield strength with radial distance is similar for all fans, the absolute values differ between fans.

These results reveal a close relationship between local fan slope and local lobe thickness. This relation suggests that local fan slope may partly set debris-flow lobe thickness, although we cannot exclude the possibility that the factors setting debris-flow lobe thickness also determine the local fan slope.

6. Conclusions

This paper evaluates fan-surface evidence for debris-flow avulsion controls and probabilities by unraveling the relative importance of (1) the superelevation of an active channel above the surrounding fan surface and (2) the formation of channel plugs that locally block a channel and force avulsion in subsequent flows. This is done by analyzing the spatial variability of debris-flow lobe and channel dimensions as well as channel-bed superelevation and avulsion locations on nine well-preserved debris-flow fans in Saline Valley, California, USA.

Channels on the study-area fans are superelevated by 2–5 channel depths above the fan surface on average, and locally by >7 channel depths. These superelevation values are greater than those observed on fluvial fans, where avulsion generally occurs once superelevation equals 0.5–1 channel depths. The large values of superelevation, its spatial variability, and the lack of a clear correlation with avulsion locations all imply that superelevation is not a good predictor of avulsion occurrence on these fans.

We show instead that channel-plug formation appears to be the dominant mechanism for triggering debris-flow avulsions. The majority of avulsions on the studied debris-flow fans were triggered by channel-plug formation, which can lead to avulsion if lobe thickness equals or exceeds channel depth. Approximately 80% of the observed channel plugs exceed the median lobe thickness at the same radial distance from the apex, on average by a factor of 1.8.

We find that both lobe and channel dimensions may vary by over an order of magnitude at any location across the fan surfaces. Spatially, channel depth and lobe thickness decrease, lobe width and lobe width/thickness ratio increase, and lobe cross-sectional area remains roughly constant with increasing distance from the fan apex. Debris-flow lobe dimensions were found to be unrelated to grain-size percentiles for particles of medium sand size and larger.

An important implication of the large variability in channel depth across a fan surface for debris-flow hazard assessment is that virtually any debris-flow deposit may induce avulsion in subsequent flows if it deposits material in the right location. The likelihood of debris-flow avulsion is a function of the combined probability of a debris-flow lobe stopping at a given location and having a thickness that approximately equals or exceeds the local channel depth. On the majority of the fans, median channel depth roughly corresponds to the 50th to 75th percentile lobe thickness, illustrating that in many areas there is a 25–50% probability that a channel plug has sufficient thickness to plug a channel and induce avulsion. The smallest measured channel depths often roughly correspond with the 10th to 25th percentile lobe thickness, implying a 75–90% probability of channel-plug formation with sufficient thickness to induce avulsion within relatively shallow channels across a fan surface. Apart from limited areas of fan-head incision, lobe thickness percentile curves generally follow channel depth curves, implying that avulsion has a similar probability at all radial distances.

Acknowledgments
The data used for this paper can be accessed at www.doi.org/10.6084/m9.figshare.7423730. We thank the Editor John Buffington, reviewer Kevin Schmidt, and an anonymous reviewer for their insightful comments that helped to strengthen this paper. T. d. H. was funded by the Netherlands Organization for Scientific Research (NWO) via Rubicon grant 019.153LW.002. A. L. D. acknowledges funding from the Institute of International Education via the Global Innovation Initiative program. The lidar data set was collected by NCALM (http://www.ncalm.org), as part of the Plate Boundary Observatory, which is operated by UNAVCO for EarthScope (http://www.earthscope.org) and supported by the National Science Foundation (EAR-0350028 and EAR-0732947; https://doi.org/10.5069/G9G44N6Q).

References

Antinao, J. L., & McDonald, E. (2013). An enhanced role for the Tropical Pacific on the humid Pleistocene–Holocene transition in southwestern North America. *Quaternary Science Reviews*, *78*, 319–341.

Beaty, C. B. (1963). Origin of alluvial fans, White Mountains, California and Nevada. *Annals of the Association of American Geographers*, *53*(4), 516–535.

Berti, M., & Simoni, A. (2007). Prediction of debris flow inundation areas using empirical mobility relationships. *Geomorphology*, *90*(1), 144–161.

Blair, T. C., & McPherson, J. G. (1994). Alluvial fans and their natural distinction from rivers based on morphology, hydraulic processes, sedimentary processes, and facies assemblages. *Journal of Sedimentary Research*, *64A*, 450–489.

Blair, T. C., & McPherson, J. G. (1998). Recent debris-flow processes and resultant form and facies of the Dolomite alluvial fan, Owens Valley, California. *Journal of Sedimentary Research*, *68*, 800–818.
Blott, S. J., & Pye, K. (2001). GRADISTAT: A grain size distribution and statistics package for the analysis of unconsolidated sediments. *Earth Surface Processes and Landforms*, *26*, 1237–1248.
Bollschweiler, M., Stoffel, M., & Schneuwly, D. M. (2008). Dynamics in debris-flow activity on a forested cone—A case study using different dendroecological approaches. *Catena*, *72*(1), 67–78.
Burchfiel, B., Hodges, K., & Royden, L. (1987). Geology of Panamint Valley-Saline Valley Pull-Apart System, California: Palinspastic evidence for low-angle geometry of a Neogene Range-Bounding Fault. *Journal of Geophysical Research*, *92*(B10), 10,422–10,426.
Carbonneau, P. E., Lane, S. N., & Bergeron, N. E. (2004). Catchment-scale mapping of surface grain size in gravel bed rivers using airborne digital imagery. *Water Resources Research*, *40*, W07202. https://doi.org/10.1029/2003WR002759
Carling, P., Gupta, N., Atkinson, P., & He, H. Q. (2016). Criticality in the planform behavior of the Ganges River meanders. *Geology*, *44*(10), 859–862.
Chen, J. H., & Moore, J. G. (1982). Uranium-lead isotopic ages from the Sierra Nevada Batholith, California. *Journal of Geophysical Research*, *87*(B6), 4761–4784.
Conrad, J. E., & McKee, E. H. (1985). Geologic map of the Inyo Mountains Wilderness Study Area, Inyo County, California (*Tech. rep.*): USGS.
Coussot, P., Laigle, D., Arattano, M., Deganutti, A., & Marchi, L. (1998). Direct determination of rheological characteristics of debris flow. *Journal of Hydraulic Engineering*, *124*(8), 865–868.
D'Arcy, M., Roda-Boluda, D. C., & Whittaker, A. C. (2017). Glacial-interglacial climate changes recorded by debris flow fan deposits, Owens Valley, California. *Quaternary Science Reviews*, *169*, 288–311.
De Haas, T., Berg, W., Braat, L., & Kleinhans, M. G. (2016). Autogenic avulsion, channelization and backfilling dynamics of debris-flow fans. *Sedimentology*, *63*, 1596–1619.
De Haas, T., Braat, L., Leuven, J. F. W., Lokhorst, I. R., & Kleinhans, M. G. (2015). Effects of debris-flow composition and topography on runout distance, depositional mechanisms and deposit morphology. *Journal of Geophysical Research: Earth Surface*, *120*, 1949–1972. https://doi.org/10.1002/2015JF003525
De Haas, T., Densmore, A. L., Stoffel, M., Suwa, H., Imaizumi, F., Ballesteros-Cánovas, J. A., & Wasklewicz, T. (2018). Avulsions and the spatio-temporal evolution of debris-flow fans. *Earth Science Reviews*, *177*, 53–75.
De Haas, T., Hauber, E., Conway, S. J., van Steijn, H., Johnsson, A., & Kleinhans, M. G. (2015). Earth-like aqueous debris-flow activity on Mars at high orbital obliquity in the last million years. *Nature Communications*, *6*, 7543.
De Haas, T., Kleinhans, M. G., Carbonneau, P. E., Rubensdotter, L., & Hauber, E. (2015). Surface morphology of fans in the high-Arctic periglacial environment of Svalbard: Controls and processes. *Earth-Science Reviews*, *146*, 163–182.
De Haas, T., Kruijt, A., & Densmore, A. (2018). Effects of debris-flow magnitude-frequency distribution on avulsions and fan development. *Earth Surface Processes and Landforms*, *43*, 2779–2793. https://doi.org/10.1002/esp.4432
De Haas, T., Ventra, D., Carbonneau, P. E., & Kleinhans, M. G. (2014). Debris-flow dominance of alluvial fans masked by runoff reworking and weathering. *Geomorphology*, *217*, 165–181.
DeGraff, J. V., Wagner, D. L., Gallegos, A. J., DeRose, M., Shannon, C., & Ellsworth, T. (2011). The remarkable occurrence of large rainfall-induced debris flows at two different locations on July 12, 2008, Southern Sierra Nevada, CA, USA. *Landslides*, *8*(3), 343–353.
Dietrich, A., & Krautblatter, M. (2017). Evidence for enhanced debris-flow activity in the Northern Calcareous Alps since the 1980s (Plansee, Austria). *Geomorphology*, *287*, 144–158. https://doi.org/10.1016/j.geomorph.2016.01.013
Dietrich, W. E., Smith, J. D., & Dunne, T. (1979). Flow and sediment transport in a sand bedded meander. *The Journal of Geology*, *87*(3), 305–315.
Dowling, C. A., & Santi, P. M. (2014). Debris flows and their toll on human life: A global analysis of debris-flow fatalities from 1950 to 2011. *Natural Hazards*, *71*(1), 203–227.
Dühnforth, M., Densmore, A. L., Ivy-Ochs, S., & Allen, P. A. (2008). Controls on sediment evacuation from glacially modified and unmodified catchments in the eastern Sierra Nevada, California. *Earth Surface Processes and Landforms*, *33*(10), 1602–1613.
Dühnforth, M., Densmore, A. L., Ivy-Ochs, S., Allen, P. A., & Kubik, P. W. (2007). Timing and patterns of debris flow deposition on Shepherd and Symmes Creek fans, Owens Valley, California, deduced from cosmogenic ^{10}Be. *Journal of Geophysical Research*, *112*, F03S15. https://doi.org/10.1029/2006JF000562
Fannin, R., & Wise, M. (2001). An empirical-statistical model for debris flow travel distance. *Canadian Geotechnical Journal*, *38*(5), 982–994.
Franke, D., Hornung, J., & Hinderer, M. (2015). A combined study of radar facies, lithofacies and three-dimensional architecture of an alpine alluvial fan (Illgraben fan, Switzerland). *Sedimentology*, *62*(1), 57–86.
Gourmelen, N., Dixon, T. H., Amelung, F., & Schmalzle, G. (2011). Acceleration and evolution of faults: An example from the Hunter Mountain–Panamint Valley fault zone, Eastern California. *Earth and Planetary Science Letters*, *301*(1), 337–344.
Griswold, J. P., & Iverson, R. M. (2008). Mobility statistics and automated hazard mapping for debris flows and rock avalanches, *Scientific Investigations Report 2007-5276*.
Hall, W. E., & McKevitt, E. N. M. Jr (1962). Geology and ore deposits of the Darwin Quadrangle, *Tech. rep.*
Harvey, A. (2011). Dryland Alluvial Fans, (3rd ed.)., *Arid zone geomorphology: Process, form and change in drylands* (pp. 333–371). Chichester: Wiley.
Helsen, M. M., Koop, P. J. M., & Van Steijn, H. (2002). Magnitude-frequency relationship for debris flows on the fan of the Chalance torrent, Valgaudemar (French Alps). *Earth Surface Processes and Landforms*, *27*(12), 1299–1307.
Hooke, R. L. (1967). Processes on arid-region alluvial fans. *The Journal of Geology*, *75*(4), 438–460.
Hubert, J. F., & Filipov, A. J. (1989). Debris-flow deposits in alluvial fans on the west flank of the White Mountains, Owens Valley, California, USA. *Sedimentary Geology*, *61*(3), 177–205.
Imaizumi, F., Trappmann, D., Matsuoka, N., Tsuchiya, S., Ohsaka, O., & Stoffel, M. (2016). Biographical sketch of a giant: Deciphering recent debris-flow dynamics from the Ohya landslide body (Japanese Alps). *Geomorphology*, *272*, 102–114.
Iverson, R. M. (1997). The physics of debris flows. *Reviews of Geophysics*, *35*(3), 245–296.
Iverson, R. M. (2003). The debris-flow rheology myth. *Debris-flow hazards mitigation: Mechanics, prediction, and assessment*, *1*, 303–314.
Iverson, R. M. (2014). Debris flows: Behaviour and hazard assessment. *Geology Today*, *30*(1), 15–20.
Iverson, R. M., Schilling, S. P., & Vallance, J. W. (1998). Objective delineation of lahar-inundation hazard zones. *Geological Society of America Bulletin*, *110*(8), 972–984.
Jakob, M. (2005). Debris-flow hazards and related phenomena, *Debris-flow hazard analysis* pp. 411–443). Verlag Berlin Heidelberg: Springer.
Jerolmack, D. J., & Mohrig, D. (2007). Conditions for branching in depositional rivers. *Geology*, *35*(5), 463–466.

Johnson, A. M. (1970). *Physical processes in geology: A method for interpretation of natural phenomena; Intrusions in igneous rocks, fractures, and folds, flow of debris and ice*. Cooper: Freeman.
Johnson, A., & Rodine, J. (1984). Debris flow. *Slope instability*, *1984*, 257–361.
Major, J. J. (1997). Depositional processes in large-scale debris-flow experiments. *The Journal of Geology*, *105*(3), 345–366.
Major, J. J., & Iverson, R. M. (1999). Debris-flow deposition: Effects of pore-fluid pressure and friction concentrated at flow margins. *Geological Society of America Bulletin*, *111*(10), 1424–1434.
McAllister, J. F. (1956). Geology of the Ubehebe Peak Quadrangle, California (Tech. rep.): USGS.
McArdell, B. W., Bartelt, P., & Kowalski, J. (2007). Field observations of basal forces and fluid pore pressure in a debris flow. *Geophysical Research Letters*, *34*, L07406. https://doi.org/10.1029/2006GL029183
McDonald, E. V., McFadden, L. D., & Wells, S. G. (2003). Regional response of alluvial fans to the Pleistocene-Holocene climatic transition, Mojave Desert, California. In E. V. McDonald, L. D. McFadden, & S. G. Wells (Eds.), *Paleoenvironments and paleohydrology of the Mojave and Southern Great Basin Deserts* (Vol. 368, pp. 189–205). Boulder: Geological Society of America Special Paper.
McDougall, S. (2016). 2014 Canadian Geotechnical Colloquium: Landslide runout analysis—Current practice and challenges. *Canadian Geotechnical Journal*, *54*(5), 605–620.
Miller, D. M., Schmidt, K. M., Mahan, S. A., McGeehin, J. P., Owen, L. A., Barron, J. A., et al. (2010). Holocene landscape response to seasonality of storms in the Mojave Desert. *Quaternary International*, *215*(1-2), 45–61.
Mohrig, D., Heller, P. L., Paola, C., & Lyons, W. J. (2000). Interpreting avulsion process from ancient alluvial sequences: Guadalope-Matarranya system (northern Spain) and Wasatch Formation (western Colorado). *Geological Society of America Bulletin*, *112*(12), 1787–1803.
Oswald, J. A., & Wesnousky, S. G. (2002). Neotectonics and Quaternary geology of the Hunter Mountain fault zone and Saline Valley region, southeastern California. *Geomorphology*, *42*(3), 255–278.
PRISM (2004). PRISM Climate Group, Oregon State University. http://prism.oregonstate.edu (created 2004)
Pederson, C. A., Santi, P. M., & Pyles, D. R. (2015). Relating the compensational stacking of debris-flow fans to characteristics of their underlying stratigraphy: Implications for geologic hazard assessment and mitigation. *Geomorphology*, *248*, 47–56.
Rice, S., & Church, M. (1996). Sampling surficial fluvial gravels; the precision of size distribution percentile sediments. *Journal of Sedimentary Research*, *66*(3), 654–665.
Rickenmann, D. (1999). Empirical relationships for debris flows. *Natural Hazards*, *19*(1), 47–77.
Roering, J. J., Mackey, B. H., Marshall, J. A., Sweeney, K. E., Deligne, N. I., Booth, A. M., et al. (2013). You are HERE: Connecting the dots with airborne lidar for geomorphic fieldwork. *Geomorphology*, *200*, 172–183.
Ross, D. C. (1967). Generalized geologic map of the Inyo Mountains region (Tech. rep.) California.
Scheidl, C., McArdell, B. W., & Rickenmann, D. (2014). Debris-flow velocities and superelevation in a curved laboratory channel. *Canadian Geotechnical Journal*, *52*(3), 305–317.
Schumm, S., Mosley, M., & Weaver, W. (1987). *Experimental fluvial geomorphology*. New York: John Wiley and Sons.
Schürch, P., Densmore, A. L., Ivy-Ochs, S., Rosser, N. J., Kober, F., Schlunegger, F., et al. (2016). Quantitative reconstruction of late Holocene surface evolution on an alpine debris-flow fan. *Geomorphology*, *275*, 46–57.
Staley, D. M., Wasklewicz, T. A., & Blaszczynski, J. S. (2006). Surficial patterns of debris flow deposition on alluvial fans in Death Valley, CA using airborne laser swath mapping data. *Geomorphology*, *74*(1), 152–163.
Stock, J. D., Schmidt, K. M., & Miller, D. M. (2008). Controls on alluvial fan long-profiles. *Geological Society of America Bulletin*, *120*(5-6), 619–640.
Stoffel, M., Conus, D., Grichting, M. A., Lièvre, I., & Maître, G. (2008). Unraveling the patterns of late Holocene debris-flow activity on a cone in the Swiss Alps: Chronology, environment and implications for the future. *Global and Planetary Change*, *60*(3), 222–234.
Suwa, H., Okano, K., & Kanno, T. (2009). Behavior of debris flows monitored on test slopes of Kamikamihorizawa Creek, Mount Yakedake, Japan. *International Journal of Erosion Control Engineering*, *2*(2), 33–45.
Suwa, H., & Okuda, S. (1983). Deposition of debris flows on a fan surface, Mt. Yakedake, Japan. *Zeitschrift fur Geomorphologie NF Supplementband*, *46*, 79–101.
Takahashi, T. (1978). Mechanical aspects of debris flow. *American Society of Civil Engineers Proceedings, Journal of the Hydraulics Division*, *104*, 1153–1169.
Ventra, D., & Nichols, G. J. (2014). Autogenic dynamics of alluvial fans in endorheic basins: Outcrop examples and stratigraphic significance. *Sedimentology*, *61*(3), 767–791.
Wasklewicz, T., & Scheinert, C. (2016). Development and maintenance of a telescoping debris flow fan in response to human-induced fan surface channelization, Chalk Creek Valley Natural Debris Flow Laboratory, Colorado, USA. *Geomorphology*, *252*, 51–65.
Whipple, K. X., & Dunne, T. (1992). The influence of debris-flow rheology on fan morphology, Owens Valley, California. *Geological Society of America Bulletin*, *104*(7), 887–900.
Wieczorek, G. F., Larsen, M., Eaton, L., Morgan, B., & Blair, J. (2001). Debris-flow and flooding hazards associated with the December 1999 storm in coastal Venezuela and strategies for mitigation: US Geological Survey. Tech. Rep. (Open File Report 01-0144).
Zaginaev, V., Ballesteros-Cánovas, J., Erokhin, S., Matov, E., Petrakov, D., & Stoffel, M. (2016). Reconstruction of glacial lake outburst floods in northern Tien Shan: Implications for hazard assessment. *Geomorphology*, *269*, 75–84.